Analyst

Cite this: *Analyst*, 2012, **137**, 5749

www.rsc.org/analyst

**PAPER**

# A bacteriophage endolysin-based electrochemical impedance biosensor for the rapid detection of *Listeria* cells

**Mona Tolba,†[a] Minhaz Uddin Ahmed,‡[a] Chaker Tlili,[a] Fritz Eichenseher,[b] Martin J. Loessner[b] and Mohammed Zourob*[a]**

***Received 20th July 2012, Accepted 19th September 2012***
**DOI: 10.1039/c2an35988j**



The objective of this study was to develop a biosensor using the cell wall binding domain (CBD) of bacteriophage-encoded peptidoglycan hydrolases (endolysin) immobilized on a gold screen printed electrode (SPE) and subsequent electrochemical impedance spectroscopy (EIS) for a rapid and specific detection of *Listeria* cells. The endolysin was amine-coupled to SPEs using EDC/NHS chemistry. The CBD-based electrode was used to capture and detect the *Listeria innocua serovar 6b* from pure culture and 2% artificially contaminated milk. In our study, the endolysin functionalized SPEs have been characterized using X-ray photoelectron spectroscopy (XPS). The integration of endolysin-based recognition for specific bacteria and EIS can be used for direct and rapid detection of *Listeria* cells with high specificity against non-*Listeria* cells with a limit of detection of $1.1 \times 10^4$ and $10^5$ CFU $mL^{-1}$ in pure culture and 2% milk, respectively.

## 1. Introduction

Detection of pathogenic bacteria has been an area of prime interest in the field of food and water safety, public health and bio-terrorism. Billions of people around the world are infected by bacteria each year.[1] *Salmonella*, *Campylobacter jejuni*, *Listeria*, *Shigella* and *Escherichia coli* are the major food and water borne pathogens which cause serious illness upon infection. *Listeria* has specifically gained much interest recently because it is one of the most virulent food-borne pathogens, with 20 to 30% mortality rate exceeding even *Salmonella* and *Clostridium botulinum*.[2,3] *Listeria* is a motile facultative anaerobe, Gram-positive intracellular bacterium. It is the third most common cause of meningitis in newborns.[4] The pathogen is found in a variety of foods including dairies worldwide and is usually present in very low number, and accompanied by a numerous and diverse background microflora. *Listeria* is conventionally detected using a plate count technique, enzyme-linked immunosorbent assay (ELISA),[5] biochemical tests and/or polymerase chain reaction (PCR),[6] flow cytometery[7] and matrix-assisted laser desorption/ionization (MALDI)[8] methods. These techniques are, however, time-consuming, labor-intensive and require pure sample. Therefore, there is a need for alternative sensitive detection methods that are able to detect low contamination levels, yield results in shortest possible time, are reliable, affordable and easy to use.[9,10]

Electrochemical impedance spectroscopy (EIS) is of great interest since it is capable of detecting small changes occurring at the solution–electrode interface in a very short time. Furthermore, EIS is simple, cost effective, and no additional reagents are necessary. Therefore, this platform enables a real-time and label-free detection of analytes binding onto surfaces.[11,12] In most recent years, EIS has been widely applied in the field of microbiology as a mean to sense and/or quantify pathogenic bacteria.[1,13–15] The integration of impedance with biological recognition technology for detection of bacteria has led to the development of impedance biosensors which substantially reduced the assay time down to ~30 min compared with the lengthy growth based methods.[13–17] The selection of an appropriate bio-recognition element and its binding strategy is the first critical step to create biosensors with improved selectivity and stability. Use of the self-assembled monolayer (SAM) and covalent binding provides options for strong and stable biomolecules immobilization in the very near vicinity of the sensor surface. Pathogen detection platforms usually employ antibodies (Abs) as recognition elements.[18] However, the drawback of using antibodies as recognition elements in a biosensor is the lack of specificity, poor separation efficiency and sensitivity.[19,20] Furthermore, production of specific antibodies is laborious, expensive, and time-consuming and they easily lose their activity when subjected to changing environmental conditions. Therefore, there is a need to explore alternative and more robust specific recognition receptors that are more resistant to

[a]*Institut National de la Recherche Scientifique (INRS) – Énergie Matériaux Télécommunications (EMT), 1650 Boulevard Lionel-Boulet, Varennes, J3X1S2, Quebec, Canada. E-mail: zourob@emt.inrs.ca; Fax: +1-450-929-8102; Tel: +1-514-228-6981*
[b]*Institute of Food, Nutrition, and Health, ETH Zurich, Schmelzbergstrasse 7, 8092 Zurich, Switzerland*
† Current address: Faculty of Veterinary Medicine, Beni-Suef University, Egypt
‡ Current address: Faculty of Science, University of Brunei Darussalam, Jalan Tungku Link, Gadong BE 1410, Brunei Darussalam

inactivation. Bacteriophages are viruses which recognise and bind to specific receptors on the host bacteria using their tail proteins. The natural ability of a phage to adsorb to, infect, and propagate within only unique host cells offers another mode of capture that can be exploited to detect, monitor and/or enumerate pathogenic bacteria. Shabani *et al.*[14] used bacteriophages as recognition receptors immobilized covalently onto screen-printed carbon electrode microarrays. The phage captured bacteria were verified by scanning electron and fluorescence microscopy. The limit of detection of their impedimetric biosensor was $10^4$ CFU $mL^{-1}$ in 50 μL sample. Mejri *et al.*[15] compared the use of antibodies and phages as bioreceptors on an interdigitated electrode for bacterial sensing, by EIS detection using phages generated successive dual signals that consisted of an initial increase in impedance caused by bacterial capture followed by a decrease in impedance due to phage-bacterial lysis. They have shown that their biosensors have a linear range between $10^4$ and $10^7$ CFU $mL^{-1}$ with a limit of detection (LOD) of $10^4$ CFU $mL^{-1}$.

Various detection formats based on *Listeria* phages have been developed such as phage typing[21] and *Listeria* detection by recombinant luciferase reporter phage.[22] Even though bacteriophages were used as recognition and binding agents for the detection of their specific targeted bacteria, their drawback was their poor capturing efficiency.[23] Endolysins from bacteriophage infecting *Listeria* are peptidoglycan hydrolases, a type of enzyme that mediates bacterial lysis at the end of the phage multiplication cycle. They are modular proteins and show a domain organization (N-terminal catalytic domain and C-terminal cell wall binding domain (CBD)).[24] The CBDs from *L. monocytogenes* phage endolysins Ply118 and Ply500 specifically recognize and bind to the *Listeria* cell wall. In addition to the recognition specificity, endolysins feature a novel and unique fold responsible for recognition of very strong binding affinity for the cognate cell wall ligands especially of the Gram-positive bacteria as they lack the outer membrane.[25] As a new and innovative approach for selective binding and separation of bacterial cells, the CBDs of bacteriophage endolysins were used for preconcentration and detection of *Listeria* cells.[24] The authors evaluated the immobilization of the CBD of endolysins on different magnetic beads for the separation and concentration of low concentrations of *Listeria*, the recovery rate was 86–99% which offered clear advantage over antibodies, which frequently show cross-reactivity with other non-target cells. The reported detection limit with pre-enrichment was 100 CFU $mL^{-1}$ and 0.1 CFU $mL^{-1}$ in 6 and 24 hours, respectively.[26] Schmelcher and his colleagues employed differently labelled reporter cell binding domains of *Listeria* phage endolysins for detection and differential staining of different *Listeria* strains. *Listeria* cells were recovered from food such as milk and soft cheeses by endolysin-magnetic concentration and separation steps. The separation was followed by plating on an Oxford agar (incubated overnight), then colonies differentiation with fluorescently labelled endolysins which led to easy staining of colony materials and their subsequent detection by fluorescence microscopy in less than 15 minutes.[27] The authors concluded that the binding of CBDs is restricted to organisms of the genus *Listeria*, it is not species specific. Instead, it correlates with the different serovars group designations; *i.e.*, CBD118 binds to *Listeria* cells of serovars 1/2, 3, and 7 and CBD500 recognizes cells of serovars 4, 5, and 6. Thus, these two CBD molecules feature non-overlapping binding ranges and cover the full diversity of different *Listeria* serovars, independent of the species or source.[24]

The present work reports on the covalent immobilization of bacteriophage endolysin CBD500 onto functionalized screen printed electrode transducer surfaces and their use for the direct/rapid impedimetric detection of *Listeria* cells in pure culture and artificially contaminated milk.

## 2. Materials and method

### 2.1. Bacteria, culture condition, and CBD500 protein (endolysin)

*L. innocua* ATCC 33091 serovar 6b and *E. coli* B (ATCC# 11303) were grown in LB medium (Oxoid) for 16–20 h at 37 °C. Cells were titered using culture plate colony count and found to be approximately $4 \times 10^9$ CFU $mL^{-1}$. For preparation of bacterial suspensions of different concentrations from the stock, 1 mL of the stock was subjected to serial dilutions in sterile phosphate buffered saline (PBS: 120 mM NaCl, 50 mM $NaH_2PO4$, pH 7.4). Recombinant endolysin consisting of 6xHis-tagged N-terminal green fluorescent protein fused to C-terminal CBD500 was obtained from Dr Martin J. Loessner Institute of Food Science and Nutrition, Switzerland. The purified protein was adjusted to 2.5 mg $mL^{-1}$ in PBS buffer and stored at −20 °C.

### 2.2. Modification of a gold electrode and assay performance

Immobilization of endolysin protein was based on the formation of self-assembled monolayers of alkanethiol group on gold electrode surfaces. A schematic diagram of the process is illustrated in Fig. 1. Briefly, the gold electrodes were preconditioned by immersing in a 1 mM ethanolic solution of 11-mercaptoundecanoic acid (MUA) for 16 h at room temperature. After preconditioning, the chip surface was completely rinsed with absolute ethanol followed by deionized water (DI) to remove any unattached species and then dried in a stream of nitrogen. The gold electrode was activated in an aqueous solution of 0.4 M (76.8 mg $mL^{-1}$ $ddH_2O$) 1-(3-dimethylaminopropyl)-3-ethylcarbodiimide (EDC) and 0.1 M (11.5 mg $mL^{-1}$ $ddH_2O$) *n*-hydroxysuccinimide (NHS) for 1 h at room temperature and washed with deionized water and dried with nitrogen. Five μL of endolysins (0.8 mg $mL^{-1}$) was added to the gold electrode and incubated at room temperature for 1 h. Then the surface was washed 3 times with PBS buffer (pH 7.4), then a 5 μL of BSA solution (0.01%) was spiked on the gold electrode and incubated for 30 minutes to prevent successive non-specific adsorption of non-targeted bio-components. This was followed by covering the gold electrode with 5 μL *Listeria innocua* suspension in PBS (pH 7.4) for 20 minutes. After rinsing with PBS for 3 times, the electrode was ready for EIS measurements. To prevent evaporation, a closed container enclosing a damp environment with soaked paper towel was used for modification of the electrodes during the functionalization procedure. In parallel to the measuring of *Listeria innocua*, a control experiment was also performed at the same time using *E. coli* B. To determine the limit of detection, ten-fold serial dilutions ($10^0$ to $10^9$ CFU $mL^{-1}$) of *Listeria* or *E. coli* were spotted over the protein modified gold electrodes.

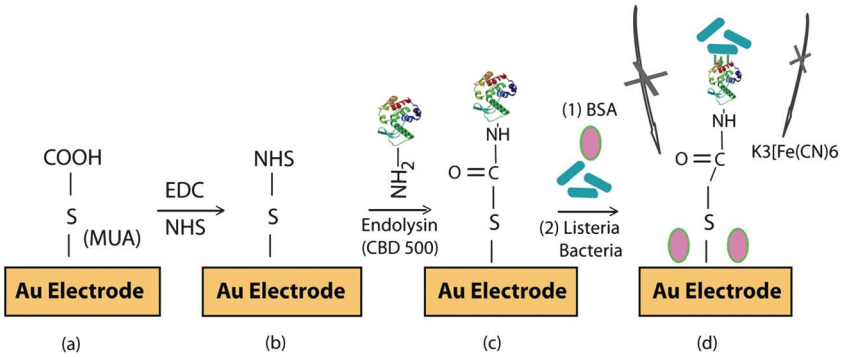


**Fig. 1** Schematic illustration of the preparation of the endolysin biosensors. Mercaptoundecanoic acid (MUA) modified gold surface (a); EDC/NHS activated MUA gold surface (b); endolysin immobilized on an activated gold sensor surface (c); followed by BSA blockage and finally assay performance with *Listeria* bacteria (d).



### 2.3. Electrochemical measurements

The electrochemical measurements were performed using three-electrode based screen printed electrochemical printed chips (Biodevice Co. Ltd. Japan) at room temperature in a convenient one compartment voltammetric potentiostat equipped with an impedance analyzer (Autolab PGSTAT 302) and acquisition software (Nova 1.6). Screen printed gold electrodes (SPE) act as working electrodes with an effective surface area of 3.67 $mm^2$. Cyclic voltammetry (CV) was carried out using the same electrodes with the potential scanned from −0.2 to +0.6 V at a scan rate of 100 mV $s^{-1}$. The impedance spectra were obtained in a frequency range from 100 mHz to 100 kHz, at the formal potential of the redox couple with a frequency modulation of 10 mV. The fitting program of AUTOLAB was used to analyze the impedance spectra using an appropriate equivalent electrical circuit. All measurements were performed in PBS buffer at pH 7.4 in the presence of 1.5 mM $Fe(CN)_6^{3-/4-}$ as a redox probe. All electrochemical measurements were performed in a Faraday cage.

### 2.4. X-ray photoelectron spectroscopy (XPS)

Endolysin immobilization onto the gold surfaces has been additionally confirmed by XPS measurements which have been performed in-house (INRS-EMT in Varennes, Quebec, Canada) with the VG Escalab220i XL instrument. The experiments were carried out using a monochromatic Al K-alpha X-ray source (1486.7 eV). The high-resolution spectrum of C 1s was recorded using a pass energy of 20 eV at a step size of 0.1 eV. Fitting of XPS peaks was performed using the Casa XPS 2.3.15 software.

### 2.5. Testing the endolysin-biosensor in milk sample matrices

Pasteurized 2% milk was purchased from a local provider and it was inoculated with different known concentrations of *Listeria innoccua*. The inoculated milk samples were then tested using the endolysin functionlized gold microelectrode and electrochemical impedance spectroscopy as previously described. Three electrodes were used for each milk sample. The uninoculated milk was used as a control.

## 3. Results and discussion

The detection of pathogenic bacteria is essential for safe and high quality food products, and is traditionally performed by culturing techniques which are reliable, but it is laborious, time-consuming and hard to be automated. Therefore timely pathogen detection is thus an essential priority for public safety. EIS is a powerful electrochemical technique capable of detecting small changes occurring at the solution–electrode interface. Accordingly, EIS was used for characterization of surface modification as well as for monitoring binding events.[15] The gold screen printed electrodes used in this study were endolysin functionalized using a self-assembling technique that has been widely used as a platform for recognition receptors immobilization due to their functionality, simplicity and flexibility.[28] The endolysin recognition receptor was covalently coupled to a MUA-modified gold electrode after the activation of the latter with EDC/NHS chemistry. The stepwise assembly of the endolysin biosensors was monitored by multi-techniques characterization using XPS, cyclic voltammetry, and EIS.

### 3.1. XPS surface characterization

XPS is used to monitor each reaction step in the endolysin immobilization on the electrode surface as it can provide information about the intermolecular bonding energy, the chemical structure of the film, the atomic concentration, and the surface contamination.[29] After the functionalization of the gold surface with carboxylic acid terminated alkanethiol self-assembled monolayers (MUA), the carboxylic acid end groups were activated with succinimide esters using EDC and NHS chemistry as shown in Fig. 1. The resulting activated layer was then used to immobilize the endolysin. XPS monitored the changes in the elemental composition of gold (Au 4d), carbon (C 1s), nitrogen (N 1s), and oxygen (O 1s) after each reaction step. Fig. 2 shows the XPS survey-spectra of the bare gold electrode (Fig. 2a) and the final modified gold electrode with endolysin proteins (Fig. 2b). The survey spectrum of the bare gold electrode shows peaks at 285 eV, 334 eV, 354 eV, and 532 eV, which are assigned to C 1s, Au 4d5/2, Au 4d3/2 and O 1s, respectively. The results are in good agreement with those reported in the literature.[30,31] The peaks of the carbon and oxygen are due to the contamination of the gold surface and this can be explained by the fact that the gold surface is able to absorb hydrocarbon contaminants from atmosphere before XPS experiments. After the alkanethiol self-assembled monolayer of 11-mercaptoundecanoic acid, activation of the COOH groups with EDC/NHS and the attachment

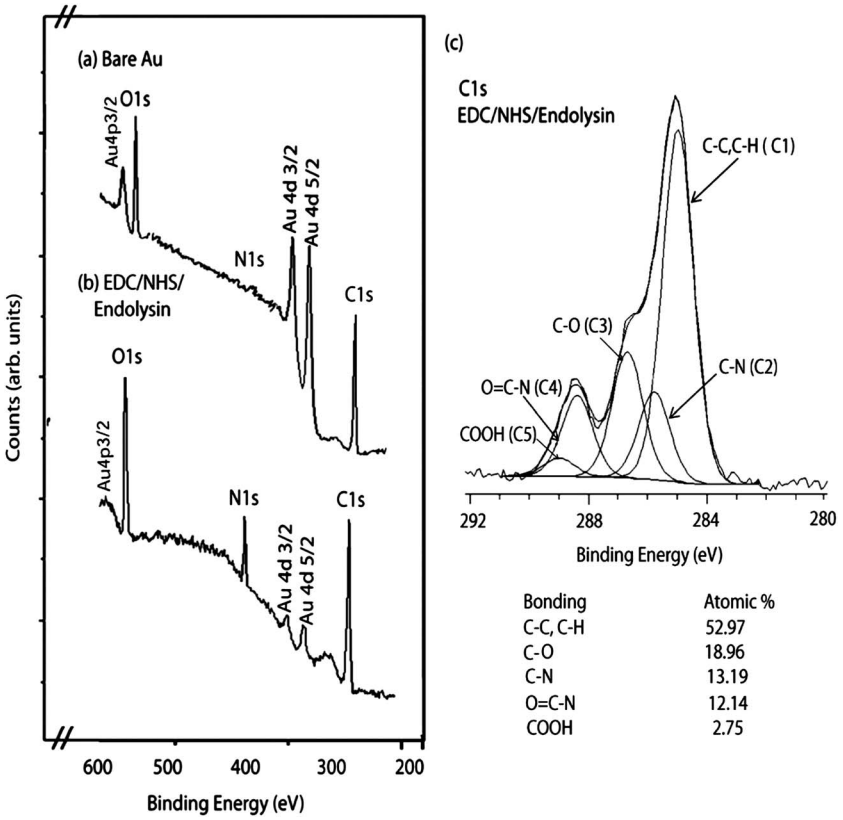


**Fig. 2** XPS survey spectra of bare Au (a) and MUA–NHS–EDC functionalized and endolysin immobilized gold electrode (b). The survey scan of the bare gold electrode shows peaks at 285 eV, 334 eV, 354 eV, and 532 eV, which are assigned to C 1s, Au 4d5/2, Au 4d3/2 and O 1s, respectively. After the alkanethiol self-assembled monolayer of 11-mercaptoundecanoic acid, activation of COOH groups with NHS/EDC chemistry and the attachment of the endolysin proteins resulted in increase in both the relative elemental compositions of carbon and oxygen on the surface and the appearance of a peak corresponding to nitrogen (b). (c) High resolution spectra of C1s in the presence of protein endolysin. The C1 represents the peak of C–C and C–H at 285 eV. The C–N peak of amines at 285.8 eV (C2) corresponds to amino acid residues lysine, arginine, histidine and tryptophan. The C–O at 286.8 eV (C3) indicates amino acid residues serine, tyrosine and threonine of endolysin. The amide bond (N–C═O) formation is shown at 288.3 eV (C4) binding energy. The peak of carboxylic acids (–COOH) at 288.8 eV (C5) represents the residues aspartic and glutamic acid of endolysin.

of the endolysin protein resulted in both increase in the relative elemental compositions of carbon and oxygen on the surface and the appearance of a peak corresponding to nitrogen (Fig. 2b). However, the Au 4d peaks are significantly attenuated by the functionalization of the bare gold electrode and the immobilization of the protein.

In Fig. 2c, the high resolution deconvoluted peaks at 286.6 eV and 288.2 eV were assigned to the amine C–N bonded carbons and the amide carbon (N–C═O) respectively of the bound endolysin. The carboxylic acid (–COOH) peak at 288.8 eV shows the presence of amino acid residues of aspartic and glutamic acid of endolysin. The C–O indicates the residues of serine, tyrosine and threonine of surface endolysin. The binding energies of these peaks are in good agreement with those observed in the literature on the XPS analysis of protein.[32–34] Before adding endolysin, the EDC/NHS modified surface was also scanned and the presence of the nitrogen 1s signal at ~402 eV was clearly observed (data not shown).

### 3.2. Cyclic voltammetry studies

Cyclic voltammetry is an efficient, well accepted analytical method and is commonly used to monitor surface modification, since it provides a rapid and simple method for initial characterization. The reversible redox couple, $Fe(CN)_6^{3-/4-}$, in 10 mM PBS, at pH 7.4, was selected as a redox probe to investigate the characteristics of the gold surface electrode in each modification step. Fig. 3A shows the cyclic voltammograms of the gold electrode in $Fe(CN)_6^{3-/4-}$ solution after different modification steps. As expected, $Fe(CN)_6^{3-/4-}$ showed a reversible behaviour on the bare screen printed gold electrode with a peak-to-peak separation of 80 mV. The covalent assembly of the MUA thiol and the activation of the COOH end groups to NHS are accompanied by a dramatical decrease in the peak current and increase in the peak-to-peak separation, which can be explained by the inhibition of the electron transfer of the redox probe at the gold surface after the formation of a tightly packed layer. After the immobilization of the endolysin protein, there is a slight decrease in the peak current and the CV curve has a flattened shape.

### 3.3. Electrochemical impedance spectroscopy studies

Fig. 3B shows the results of Faradic impedance spectroscopy on the bare gold electrode, the activated MUA-modified gold electrode with EDC/NHS, and the endolysin proteins immobilization on the activated surface, in the presence of the redox couple

 

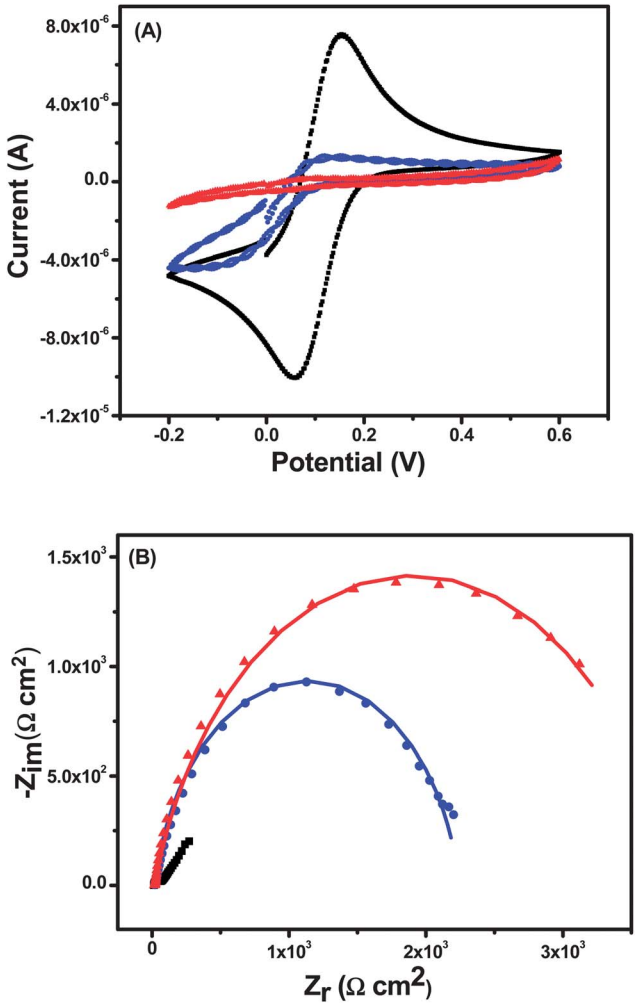


**Fig. 3** Cyclic voltammetry (A), and the Nyquist plot (B) of the bare screen printed gold electrode (SPE) (■), the MUA-EDC-NHS functionalized-SPE (●), and the immobilized endolysin proteins (▲) in the presence of 1.5 mM $Fe(CN)_6^{3-/4-}$ in 10 mM of PBS (pH 7.4). Impedance spectra were acquired at the formal potential of $Fe(CN)_6^{3-/4-}$ in the $10^5$ to 0.1 Hz frequency range. The symbols represent the experimental data and the solid curves represent the fitted data using the equivalent circuit in Fig. 4A.

$Fe(CN)_6^{3-/4-}$ measured at the formal potential of the redox couple. The formal potential value of 100 mV was determined from the cyclic voltammetry curve of the bare gold screen printed electrode. This value was in agreement with the value reported by Lucarelli *et al.*[35] The impedance plot of the bare gold electrode is characterized by a small semi-circle at high frequency domain, which corresponds to an interfacial charge transfer mechanism, and followed by a low-frequency Warburg line with the slope near the unity, which corresponds to the domination of the mass diffusion effects over the electron transfer process. The semicircle corresponds to a parallel combination of the charge-transfer resistance, $R_{ct}$, with the double layer capacitance, $C_{DL}$, while the linear response is related to mass transport effects. In order to determine the electrical parameters of the bare gold electrode, the impedance spectra of the bare gold electrode were fitted with the slightly modified Randles equivalent circuit (Fig. 4A). This circuit includes the background solution resistance, $R_s$, the

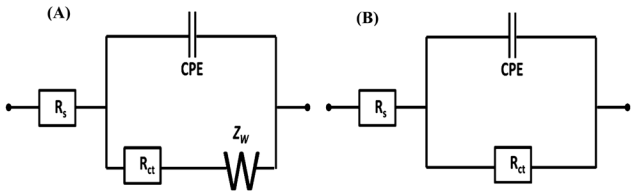


**Fig. 4** Illustration of the equivalent circuit used in this work. Equivalent circuit for the bare gold electrode (A) and equivalent circuit for the modified gold electrode (B).

charge-transfer resistance, $R_{ct}$, the Warburg impedance, $Z_W$, resulting from the diffusion of the redox couple from the bulk of the solution to the electrode interface, and the constant phase element (CPE) represents the electrical double-layer capacitance, resulting from the surface irregularities of the gold electrode and the inhomogeneity of the current distribution.[11] The impedance of the CPE is given by the following equation:

$$Z_{CPE} = 1/Q_0(j\omega)^{\alpha}$$

where $\omega$ is the electric field frequency, $Q_0$ is the modulus of the constant phase element, measured in Farads $cm^{-2}$ $s^{\alpha-1}$, and the exponent $\alpha$ varies from 0 to 1 and reflects the ideality of the capacitor.[36] For example, when $\alpha$ equals 1.0, the CPE is an ideal capacitor. The $R_s$ and $Z_W$ represent bulk properties of the electrolyte solution and diffusion features of the redox probe and ions in solution. These two components are not affected by chemical modification occurring at the electrode surface. On the other hand, the $R_{ct}$ and CPE depend on the dielectric and insulating features at the electrode/electrolyte interface. For Faradic impedance measurement, the $R_{ct}$ is the most sensitive and straightforward parameter that can be used to characterize the events occurring on the surface of the working electrode. Moreover, the variation in CPE is almost unnoticeable compared to the change in $R_{ct}$. The experimental data for the bare screen printed gold electrode fit perfectly the circuit model 1 (Fig. 4A) from which very precise values were obtained for the $R_{ct}$ (47.2 Ω $cm^2$) and CPE (29.2 μF $cm^{-2}$ $s^{\alpha-1}$, $\alpha = 0.894$) with a small fit error ($\chi^2 \sim 10^{-3}$). It is shown that the CPE can be attributed to a pure capacitor because the $n$ value was basically close to 1 and it is in good agreement with the value of 25 μF $cm^{-2}$ reported by Tlili *et al.*[37] After dipping the bare screen printed gold electrode in 1 mM of MUA solution for 16 h at room temperature, and activating the COOH end groups with EDC/NHS chemistry, the diameter of the semi-circle corresponding to the charge transfer resistance is significantly increased. The reason might be due to the physical barrier of the assembled layer that prevents the access of the redox couple. It can also be noticed that the low-frequency Warburg line is no more apparent, and this observation can be explained by the low current involved in the redox reaction after functionalization of the gold surface with MUA. Therefore, the Warburg impedance can be excluded from the previous equivalent circuit and therefore we have used for the further fitting a modified Randles circuit (Fig. 4B). We found that this modified equivalent fits very well the experimental data. By fitting the data to the equivalent circuit in Fig. 4B, the charge transfer resistance exhibits a much higher value (2.2 kΩ $cm^2$) compared to the bare gold electrode. As shown in Fig. 3B, after

the immobilization of the endolysin proteins we observed a further increase in the charge transfer resistance $R_{ct}$ (3.7 kΩ cm$^2$) because of an additional barrier created towards the access of the redox probe to the electrode surface.

Fig. 5A illustrates the complex impedance response of the endolysin-modified gold screen printed in 10 mM of PBS with 1.5 mM of $Fe(CN)_6^{3-/4-}$ in the absence and presence of *Listeria* cells. To fit the experimental data we have used the same equivalent circuit presented previously in Fig. 4B. It is obvious that the charge transfer resistance $R_{ct}$ value shows a dependence upon the concentration of the *Listeria* cells, ranging from $10^4$ to $10^9$ CFU mL$^{-1}$. It can be clearly seen that the charge transfer resistance $R_{ct}$ increased (128.8%) from 3.7 kΩ cm$^2$ in the absence of the *Listeria* cells to a value of 8.5 kΩ cm$^2$ in the presence of $10^8$ CFU mL$^{-1}$. The increase in the $R_{ct}$ can be explained by the binding of the *Listeria* cells onto the immobilized endolysin proteins. This capture of the *Listeria* cells creates a physical barrier for the electrochemical process of the redox couple which can increase the charge transfer resistance. This observation is in agreement with the results reported by Yang and Li[38] that the capturing of the bacteria cells on the modified electrode surface can block the electric current flow, thereby increasing the charge transfer resistance $R_{ct}$. In order to estimate the reproducibility of our biosensors, a series of four repetitive measurements of the sample containing $10^8$ CFU mL$^{-1}$ of *Listeria* cells were carried out. The relative standard deviation (RSD) value for the impedimetric response was calculated to be 5.8% ($n = 4$).

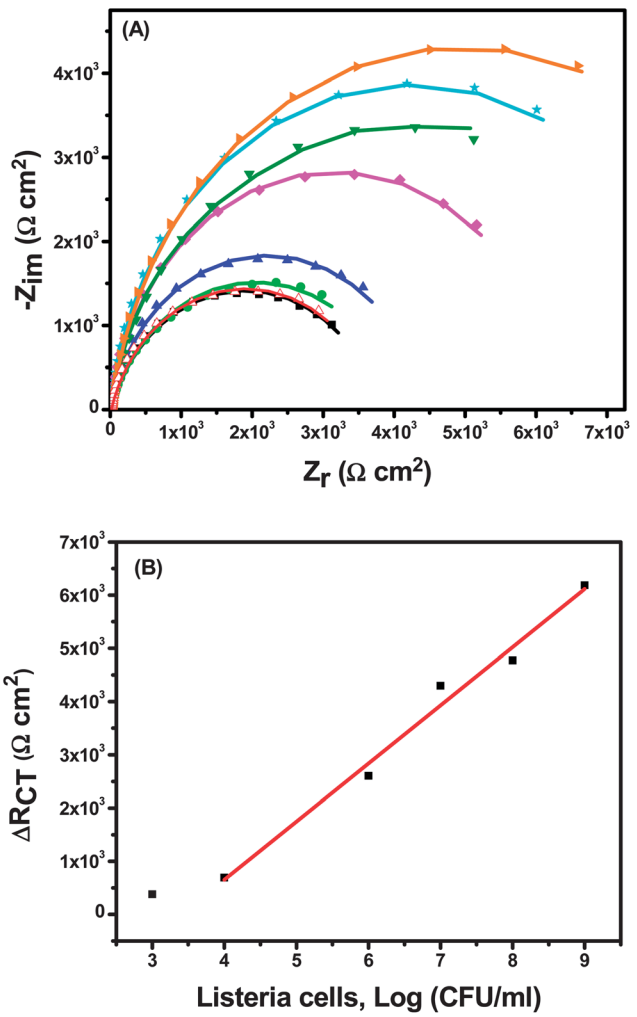


**Fig. 5** (A) Nyquist plot of the *Listeria* biosensor with increasing concentrations of *Listeria*: 0 CFU mL$^{-1}$ (■), $10^3$ CFU mL$^{-1}$ (●), $10^4$ CFU mL$^{-1}$ (▲), $10^6$ CFU mL$^{-1}$ (◆), $10^7$ CFU mL$^{-1}$ (▼), $10^8$ CFU mL$^{-1}$ (*) and $10^9$ CFU mL$^{-1}$ (►) of *Listeria* bacteria and $10^6$ CFU mL$^{-1}$ (△) of *E. coli* bacteria (A). Impedance spectra were acquired at the formal potential of $Fe(CN)_6^{3-/4-}$ *vs.* (Ag/AgCl) in PBS (pH 7.4) electrolyte in the presence of 1.5 mM $Fe(CN)_6^{3-/4-}$. The symbols are the experimental data, and the solid lines are results from the fitting of the data using the equivalent circuit in (B). A calibration plot of the *Listeria* biosensor in PBS (B).

Fig. 5B shows a calibration line of the *Listeria* biosensor in PBS. Charge transfer resistance variation $\Delta R_{ct}$ and the logarithmic value of the *Listeria* cells concentration in the range of $10^4$ to $10^9$ CFU mL$^{-1}$ exhibit a linear relationship with a slope of 1.1 kΩ cm$^2$ and a correlation coefficient of 0.98. The limit of detection (LOD) = $3S_D/m$ was $1.1 \times 10^4$ CFU mL$^{-1}$ in PBS, where $m$ is the slope of the linear part of the calibration plot and $S_D$ is the standard deviation of the blank measurement.

For successful application, the biosensors should be selective and specific for the target analyte. As shown in Fig. 6, the charge transfer resistance $R_{ct}$ increased 5%, 3.4%, and 2.8 upon incubating the biosensors with $10^3$, $10^6$, and $10^7$ CFU mL$^{-1}$ of *E. coli* cells respectively, which can be attributed to the non-specific adsorption of such bacteria cells onto the biosensor surface. An additional experiment was performed with a negative control in which the procedure shown in Fig. 1 was followed except that the endolysin proteins step was omitted. No significant increase in the charge transfer resistance $R_{ct}$ was observed (4.3%) upon exposure of the modified electrode to the large concentration of *Listeria* cells (data not shown). This indicates that the developed endolysin coated biosensor has a potential for specific detection of the *Listeria* cells.

In order to verify the ability of the biosensor to detect *Listeria* cells in a complex biological matrix such as milk, the detection of the *Listeria* cells was evaluated in 2% milk (Fig. 7). It can be clearly observed that after incubation of the endolysin-modified electrode in 2% milk there is an increase (38.5%) from 5.7 kΩ cm$^2$ to 7.9 kΩ

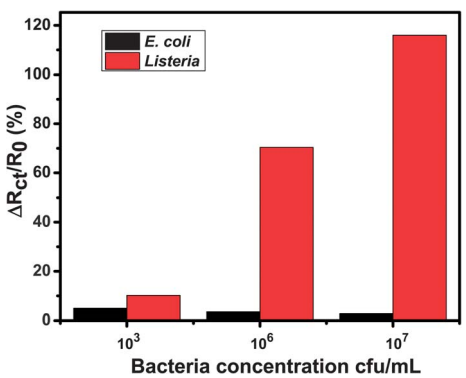


**Fig. 6** Comparison of $R_{ct}$ changes of the impedometric endolysin based biosensor to different concentrations of *E. coli* and *Listeria* cells to verify the specificity of the endolysin biosensor. $\Delta R_{ct}$ is the change of charge transfer resistance of the sensor before and after incubation with different concentrations of bacteria.

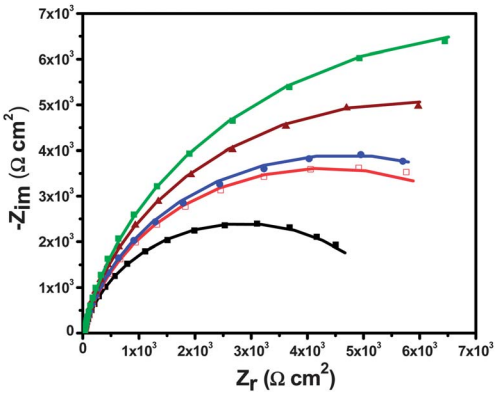


**Fig. 7** Nyquist plot of *Listeria* biosensors in 2% milk: endolysin protein-modified electrode in PBS (■), endolysin protein-modified electrode in 2% milk in the absence of *Listeria* cells (□), $10^5$ CFU $mL^{-1}$ (●), $10^6$ CFU $mL^{-1}$ (▲), and $10^8$ CFU $mL^{-1}$ (■). Impedance spectra were acquired at the formal potential of $Fe(CN)_6^{3-/4-}$ *vs.* (Ag/AgCl) in PBS (pH 7.4) electrolyte in the presence of 1.5 mM $Fe(CN)_6^{3-/4-}$. The symbols are the experimental data, and the solid lines are results from the fitting of the data using the equivalent circuit in Fig. 4B.

$cm^2$ in $R_{ct}$. It is well expected that this variation in the charge transfer resistance is due to the fact that the milk has a very complex chemical composition containing over 100 000 different molecular species, including saturated fats, proteins, vitamins and ions. Therefore, the non-specific binding can be significant in the milk-derivative samples and it is primarily due to the electrostatic attraction between the chemical composition of the milk and some residual $COO^-$ end groups at the surface of the biosensor which are proved by our XPS measurement. Our results are in agreement with Shrikrishnan and Lakshminarayanan[39] who were able to analyze the interactions of different redox probes (ferrocyanide, ferrocene, and hexaammineruthenium) with some of the constituents in the milk, especially the fat globules, their membrane, casein micelles, whey proteins and minerals. The authors recently provided an insight which suggested that there is in fact interaction between the milk fat globular membrane, the ferricyanide and the gold electrode surface while in the case of hexaammineruthenium, the more positively charged species mostly interact due to the presence of negatively charged species like casein micelles and phospholipid head groups. However, when $10^5$, $10^6$, and $10^8$ CFU $mL^{-1}$ of *Listeria* spiked in 2% milk, the charge transfer resistance increased from 7.9 kΩ $cm^2$ to 9.3, 11.9, and 15.6 kΩ $cm^2$, respectively.

The detection approach described herein has been shown to be fast and efficient in comparison with other phage-endolysin based methods reported for *Listeria* detection. For example, the methods described by Kretzer *et al.*, 2007 and Schmelcher *et al.*, 2010 are either time consuming requiring 6–24 hours of enrichment[26] and/or requiring fluorescence labeling.[27] We have a more rapid assay readout compared to the official standard surface plating which requires 96 hours of enrichment. The detection limits in this study using the endolysin-EIS for *Listeria* bacteria detection in buffer and artificially contaminated milk sample were in agreement with the previously reported phage-based detection limit ($10^4$ CFU $mL^{-1}$ for 50 μL samples) reported by Shabani *et al.*, 2008, and Mejri *et al.*, 2010, despite changing the binding/capturing/biorecognition element on the sensor surface.[14,15]

## 4. Conclusion

In the present work, low cost, label-free and robust screen printed gold electrodes have been used as the base transducers for successful immobilization of endolysin of *Listeria* bacteriophages, to act as a specific binding/recognition element for the detection of *Listeria* cells. The impedance measurements performed with these electrodes have been shown to provide a simple, rapid and direct means of detecting specific bacteria. The Nyquist plots showed significant changes in the electron transfer resistance due to endolysin immobilization and its specific binding to *Listeria* cells. A linear relationship between the electron transfer resistance and cell concentration was found in a range of bacterial concentrations from $10^4$ to $10^8$ CFU $mL^{-1}$. Furthermore, *Listeria* detection was also possible in food such as milk with a detection limit of $1.1 \times 10^4$ and $10^5$ CFU $mL^{-1}$ in pure culture and milk, respectively.

## Acknowledgements

The authors would like to express their great appreciation to the Natural Sciences and Engineering Research Council of Canada (NSERC) and NanoQuebec for their financial support.

## References

1 L. Yang and R. Bashir, *Biotechnol. Adv.*, 2008, **26**, 135–150.
2 V. Ramaswamy, V. M. Cresence, J. S. Rejitha, M. U. Lekshmi, K. S. Dharsana, S. P. Prasad and H. M. Vijila, *J. Microbiol., Immunol. Infect.*, 2007, **40**, 4–13.
3 P. Mook, S. J. O'Brien and I. A. Gillespie, *Emerging Infect. Dis.*, 2011, **17**, 38–43.
4 C. Genigeorgis, M. Carniciu, D. Dutulescu and T. B. Farver, *J. Food Prot.*, 1991, **54**, 662–668.
5 N. S. Hobson, I. Tothill and A. P. F. Turner, *Biosens. Bioelectron.*, 1996, **11**, 455–477.
6 J. L. Bailey, *J. Food Prot.*, 1998, **61**, 792–795.
7 M. Ikeda, Y. Nobuyasu and N. Masao, *J. Health Sci.*, 2009, **55**, 851–856.
8 E. Carbonnelle, J. L. Beretti, S. Cottyn, G. Quense, P. Berche, X. Nassif and A. Ferroni, *J. Clin. Microbiol.*, 2007, **45**, 2156–2161.
9 A. Subramanian, J. Irudayaraj and T. Ryan, *Biosens. Bioelectron.*, 2006, **21**, 998–1006.
10 M. Zourob, S. Elwary and T. Anthony, *Electroanalysis*, Springer Science, New York, 2008.
11 J. S. Daniels and N. Pourmand, *Electroanalysis*, 2007, **19**, 1239–1257.
12 O. Panke, T. Balkenhohl, J. Kafka, D. Schafer and F. Lisdat, *Adv. Biochem. Eng./Biotechnol.*, 2008, **109**, 195–237.
13 L. Yang, Y. Li, C. L. Griffis and M. G. Johnson, *Biosens. Bioelectron.*, 2004, **19**, 1139–1147.
14 A. Shabani, M. Zourob, B. Allain, C. A. Marquette, M. F. Lawrence and R. Mandeville, *Anal. Chem.*, 2008, **80**, 9475–9482.
15 M. B. Mejri, H. Baccar, E. Baldrich, F. J. Del Campo, S. Helali, T. Ktari, A. Simonian, M. Aouni and A. Abdelghani, *Biosens. Bioelectron.*, 2010, **26**, 1261–1267.
16 C. Ruan, H. Wang, L. Yang and Y. Li, *J. Rapid Methods Autom. Microbiol.*, 2003, **11**, 11–22.
17 S. M. Radke and E. C. Alocilja, *Biosens. Bioelectron.*, 2005, **20**, 1662–1667.
18 H. L. Grossman, W. R. Myers, V. J. Vreeland, R. Bruehl, M. D. Alper, C. R. Bertozzi and J. Clarke, *Proc. Natl. Acad. Sci. U. S. A.*, 2004, **101**, 129–134.
19 G. Duffy, J. Sheridan, H. Hofstra, D. A. McDowell and I. S. Blair, *Lett. Appl. Microbiol.*, 1997, **24**, 445–450.
20 E. Kaclikova, T. V. Kuchta, H. Kay and D. Gray, *J. Microbiol. Methods*, 2001, **46**, 63–67.
21 M. J. Loessner and M. Busse, *Appl. Environ. Microbiol.*, 1990, **56**, 1912–1918.

22 M. J. Loessner, C. E. Rees, G. S. Stewart and S. Scherer, *Appl. Environ. Microbiol.*, 1996, **62**, 1133–1140.
23 A. R. Bennett, G. C. Davids, S. Vlahodimou, J. G. Banks and R. B. Betts, *J. Appl. Microbiol.*, 1997, **83**, 259–265.
24 M. J. Loessner, K. Kramer, F. Ebel and S. Scherer, *Mol. Microbiol.*, 2002, **44**, 335–349.
25 M. J. Loessner, *Curr. Opin. Microbiol.*, 2005, **8**, 480–487.
26 J. W. Kretzer, L. Rainer, S. Mathias, B. Manuel, K. Kwang-Pyo, K. Corinna and J. L. Martin, *Appl. Environ. Microbiol.*, 2007, **73**, 1992–2000.
27 M. Schmelcher, T. Shabarova, M. R. Eugster, F. Eichenseher, V. S. Tchang, M. Banz and M. J. Loessner, *Appl. Environ. Microbiol.*, 2010, **76**, 5745–5756.
28 X. Zhang, H. Chen and H. Zhang, *Chem. Commun.*, 2007, 1395–1405.
29 S. J. Xiao, M. Textor and N. D. Spencer, *Langmuir*, 1998, **14**, 5507–5516.
30 A. N. Mansour, *Surf. Sci. Spectra*, 1994, **3**, 197–202.
31 L. He, L. Demeng, W. Yanping, X. Yinghong and C. H. Jianfei, *Colloids Surf., B*, 2011, **87**, 273–279.
32 T. N. Brack, R. Lamb, D. Pham and P. Turner, *Surf. Interface Anal.*, 1996, **24**, 704–710.
33 Y. C. Tyan, J. D. Liao, S. B. Jong, P. C. Liao, M. H. Yang, Y. W. Chang, R. Klauser, M. Himmelhaus and M. Grunze, *J. Mater. Sci.: Mater. Med.*, 2005, **16**, 135–142.
34 F. Yi, Q. Li, Z. X. Guo and J. Yu, *J. Appl. Polym. Sci.*, 2006, **99**, 1340–1345.
35 F. Lucarelli, G. Marrazza and M. Mascini, *Biosens. Bioelectron.*, 2005, **20**, 2001–2009.
36 J. R. Macdonald, *Impedance Spectroscopy*, Wiley, New York, 1987.
37 C. Tlili, N. Jaffrezic-Renault, C. Martelet, J. P. Mahy, S. Lecomte, M. M. Chehimi and H. Korri-Youssoufi, *Mater. Sci. Eng., C*, 2008, **28**, 861–868.
38 L. Yang and Y. Li, *Biosens. Bioelectron.*, 2005, **20**, 1407–1416.
39 S. Shrikrishnan and V. Lakshminarayanan, *J. Colloid Interface Sci.*, 2012, **370**, 124–131.



 